THE EVOLUTION OF SUBSURFACE MICRO-STRUCTURE AND TRIBO-CHEMICAL PROCESSES IN CoCrMo-Ti6Al4V FRETTING-CORROSION CONTACTS: WHAT LIES AT AND BELOW THE SURFACE?

Abstract

Titanium and its alloys are attractive biomaterials because of their desirable corrosion, mechanical, biocompatibility and osseointegration properties. Ti6Al4V alloy in particular remains a prominent biomaterial used in Total Hip Arthroplasty (THA). Recently, researchers have shown interest in understanding the degradation mechanisms and the subsurface implications of fretting-corrosion at the modular taper interface in THA. The purpose of this study was to utilise advanced microscopy and spectroscopy to characterise *in-vitro* fretting-corrosion induced subsurface refinement and microstructural changes in Ti6Al4V alloy. *In-vitro* fretting-corrosion tests were carried at four displacement: ±10, ±25, ±50 and ±150 µm for a CoCrMo – Ti6Al4V ball-on-flat material couple. Subsequently, high resolution micrographs of the alloy microstructure were obtained using the Transmission Electron Microscope (TEM) together with Energy Dispersed X-Ray spectroscopy (EDX). The degree of subsurface microstructural changes was observed to be linked to the slip regime and magnitude of energy dissipated at the interface. Strain-induced orientation were observed at the stick regime. The mixed and gross-slip regimes were both characterised with mechanical mixing and formation of nano-crystalline structures. Specific to the mixed fretting regime, fluid ingression and material entrapment at the interface led to further refinement of nano-crystalline structures which resulted in the formation of an amorphous Ti6Al4V structure. The interwoven relationship between energy dissipation, contact condition and mechanisms of clinical failure in Ti6Al4V alloy are discussed.

Keywords: Ti6Al4V, CoCrMo, Fretting regimes, Strain-induced orientation, Mechanical mixing, Nano-crystalline, Amorphous Ti6Al4V

1. Introduction

Modular taper interfaces are ubiquitous in modern THA. Ti6Al4V-CoCrMo alloy combinations are common at the head – neck and/or neck – stem taper interfaces. Despite the alloys being known for its good corrosion resistance, micro-motions at these interfaces result in the disruption of the protective oxide layer leading to accelerated corrosion and degradation at the interface [1-6]. This is technically known as fretting-corrosion and remains a relevant topic of discussion today. The mechanisms of fretting-corrosion, the combined action of mechanical wear and electrochemical processes in a conductive aqueous environment, were established in the early 1950s by Uhlig et al [7]. Within the area of biomaterials, fretting-corrosion damage in THA is sometimes known as Mechanically Assisted Crevice Corrosion (MACC) [8]. The mechanism broadly unifies the influence of

fretting, localised corrosion, local changes in chemistry of the physiological solution at the modular taper interface. Fretting-corrosion is a multifactorial problem that is influenced by patient factors (i.e. weight, biomechanics); surgical factors such as assembly force, component mismatch and implant factors such as material combinations and taper design [9-14].

The combination of CoCrMo femoral heads with Ti-alloy femoral stems via a modular taper connection is common practice in orthopaedics. The superior biocompatibility and lower elastic modulus (closer to bone) of Ti-alloys and enhanced wear resistance of the CoCrMo alloy drives the use of these materials for their respective applications. Ti-alloys have been implicated in several fretting and corrosion degradation mechanisms observed on modular THA. These include gross wear, imprinting, material transfer, selective dissolution of the β-phase, the promotion of degradation of the CoCrMo surface and hydrogen embrittlement [15-19]. In other more severe cases, components made from Ti6Al4V experienced *in vivo* fracture [20-22]. Moreover when used in a metal on metal total hip replacement scenario, unacceptably high revisions rates have been observed due to adverse reactions to metal debris (ARMD) owing to degradation at the modular CoCrMo-Ti-alloy modular taper interfaces [23]. In such cases the CoCrMo alloy unexpectedly shows more degradation than the 'softer' titanium counter-face and has been attributed to a fretting fatigue or tribocorrosion mechanism. Similar observations have also been seen for bi-modular hip implant systems [24].

Fretting-corrosion at mixed-metal interfaces and the roles of dynamic and time dependent subsurface microstructural changes are not fully understood. This is further complicated by the nature of the modular taper interface where the contact mechanics and degradation mechanism will vary spatially owing to their geometry and biomechanical loading [24]. It is therefore important to understand the metallurgical effects of specific contact conditions on a biomaterial during *in-vivo* fretting. So far, there are only two studies that have employed the use of advanced microscopy techniques such as the Transmission Electron Microscope (TEM) to characterise fretting-induced subsurface refinement and microstructural al changes in retrieved CoCrMo alloy and TMZF modular taper components [24, 25]. The purpose of this study was to understand the link between fretting-corrosion regime and evolution of the subsurface microstructure and tribochemical processes occurring at the interface via controlled experimentation. To achieve this, advanced microscopy, spectroscopy and nano-mechanical techniques have been employed to examine the surfaces from the nanometre scale to the macro-scale. The observations presented in this study provide further insight into the clinical observations and current engineering debate: why softer Ti alloys results in higher degradation of the harder CoCrMo alloys.

2. Materials and Methodology

2.1. Materials

A ball-on-flat configuration was utilised in this study to achieve an initial Hertzian point contact for a CoCrMo – Ti6Al4V material combination. The ball component was a wrought low-carbon Co-28Cr-6Mo (CoCrMo) while the flat component was made of wrought Extra Low Interstitial (ELI) Ti6Al4V alloy. The CoCrMo alloy was a polished ø28 mm femoral head component with surface roughness (R_a) < 10 nm. Subsequently, the Ti6Al4V flats were ground using silicon carbide grinding paper and polished using a 3 μm diamond paste down to R_a < 20 nm. Both CoCrMo and Ti6Al4V alloys were manufactured according to ASTM F 1537-11 and ASTM F 136-13, respectively, and were both supplied by Peter Brehm, Germany. All tests were conducted in 25 % volume Foetal Bovine Serum (FBS, SeraLab, USA) diluted with Phosphate Buffered Saline (PBS) and 0.03% volume Sodium Azide (SA) was added to retard bacteria growth.

2.2. Fretting-corrosion simulation

Fig 1 shows an image and schematic of the experimental set-up. Further details on the tribometer are presented in a previous study [1]. The image shows a delrin bath in which 12 mL of simulated physiological solution was placed. The temperature was kept at 37±2 °C using thermostatically controlled hot water circulation within the delrin bath as shown in Fig 1. A 3-electrode electrochemical cell was integrated into the fretting tribometer consisting of the tribo-couple as the working electrode (WE) and a combination Ag/AgCl reference electrode (RE) and Pt counter electrode (CE) (ORP Redox, Orion 9179, Thermoscientific, USA). The open circuit potential (OCP) was measured as a semi-quantitative indication of corrosion at the interface, with a decrease in OCP at the start of sliding indicative of de-passivation processes. The OCP was measured at a frequency of 1 Hz using a PGSTAT101 (Autolab, NV)
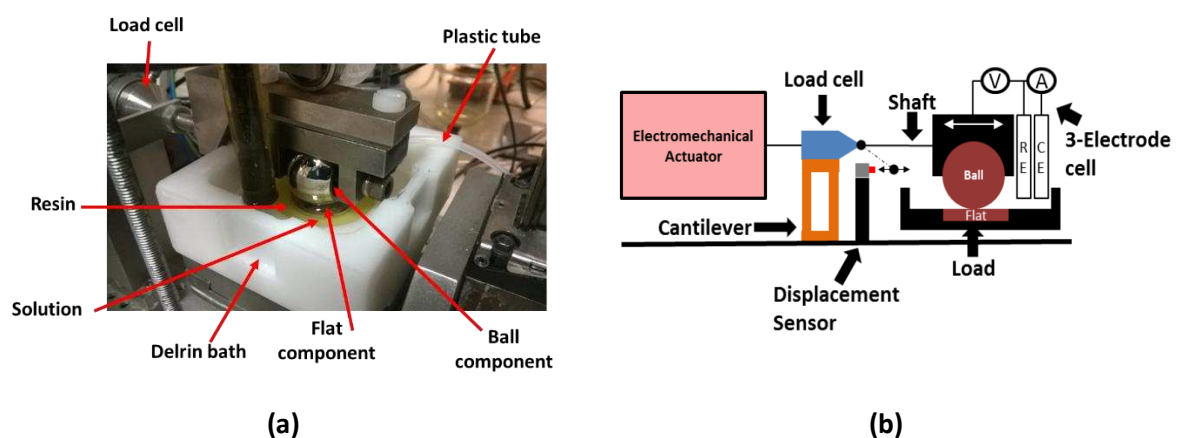

(a)   **(b)**

Fig 1 - a) An image of the fretting corrosion set-up and b) schematic representation of the fretting-tribometer used in this study.

Four fretting displacement amplitudes (δ_d) were assessed: ±10, ±25, ±50 and ±150 µm. These were chosen with the aim of assessing systematic subsurface refinement and microstructural al changes in Ti6Al4V at various fretting regimes. An initial maximum Hertzian contact pressure of 1 GPa (F_n = 120N) was used for all fretting tests in this study and each fretting test lasted 6000 cycles at a frequency of 1 Hz. High contact pressures are conceivable at these interfaces particularly at the neck – stem modular taper and during severe loading conditions such as stumbling [13, 26]. The criteria as given by Fouvry et al [27, 28] was used to characterise the nature of slip at the fretting-corrosion interfaces. After fretting-corrosion surfaces were removed from the test, lightly rinsed with de-ionised water to remove any loose debris and dried under an N_2 stream.

2.3. Vertical Scanning Interferometry (VSI)

The total material lost from the fretting contact of the ball and flat components was measured using a NPFLEX interferometer (Bruker, USA). Surfaces were scanned, corrected for curvature or Sphericity (in the case of the CoCrMo ball) and the volumes losses / gains determined using the Vision64 software (Bruker, USA). Fig 2 shows a schematic of the surface evaluation using VSI analysis. Negative (V^-) and positive (V^+) volume losses were determined about a reference zero-axis determined from areas not subjected to tribocorrosion.
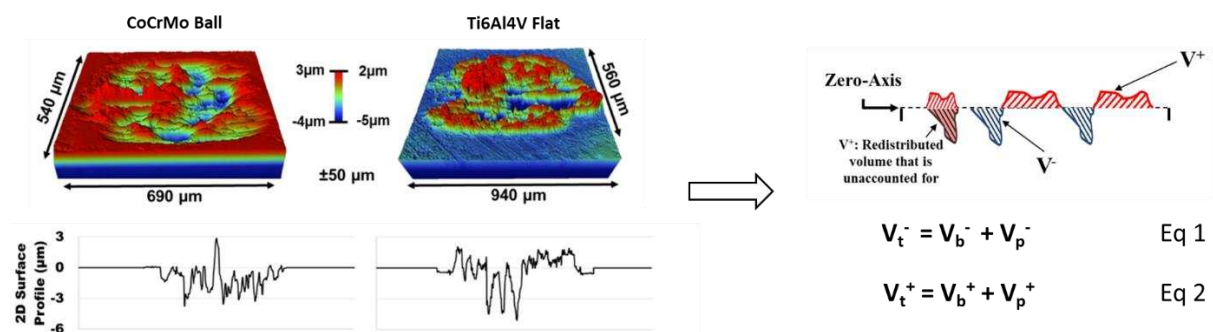

Fig 2 – Schematic representation of the determination of wear from the CoCrMo ball and Ti6Al4V surface after fretting corrosion where V_b^- and V_p^- are volume losses for the ball and plate, respectively. V_b^+ and V_p^+ represent volume gains for the ball and plate, respectively.

2.4. Transmission Electron Microscopy (TEM)

The subsurface refinement and microstructural changes of the Ti6Al4V alloy were characterised using TEM to obtain high resolution micrographs. The samples were prepared using the FEI Nova200 FIBSEM equipped with a Kleindiek micro-manipulator Focused Ion Beam (FIB). This was done following an established method outlined in a previous study by Bryant et al [29]. The region of interest of the Ti6Al4V surface was protected from ion-beam damage by coating with two layers of Platinum (Pt). Fig 3 shows a schematic diagram of a typical wear scar for three fretting regimes and illustrates the

composite contact conditions that typically exists at a fretting interface. A benefit of the ball-on-flat contact is that defined slip regimes can be easily identifiable. It is expected that the extent of microstructural variations incurred within the alloy would be site specific. TEM samples were obtained from a consistent region for all samples i.e. from an annulus nearer to the edge of the contact boundary as depicted in Fig 3. In all cases the TEM samples removed were orthogonal to the direction of the fretting axis. A TEM sample not subjected to fretting-corrosion was obtained from polished Ti6Al4V surface and taken as a reference microstructure. TEM samples were analysed using a FEI Tecnai F20 FEGTEM (200 kV) fitted with a Gatan Orius SC600 CCD camera running GMS1 software and an Oxford Instruments 80 mm^2 EDS SDD running AZtec software. Bright-field, dark-field and Selected Area Electron Diffraction (SAED) patterns were all captured using the digital camera, and scanning TEM (STEM)-EDX mapping was carried out while imaging in high angle annular dark field (HAADF) mode at magnifications of 7000 and 28000 X. An approximately 10 nm probe was used, and maps were collected for approximately 10 minutes. The contrast between bright and dark regions in the TEM micrograph are indicative of different crystal orientations.
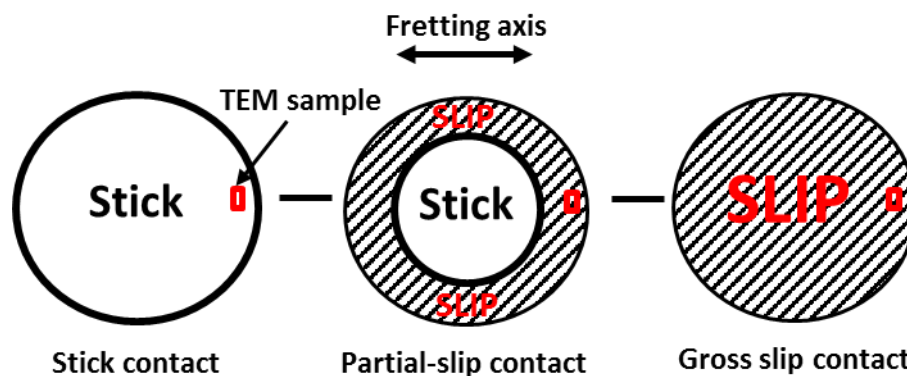

Fig 3 - A schematic diagram of fretting wear scars corresponding to different fretting regimes.

3. Results

3.1. Open circuit potential

Fig 4a shows the evolution of OCP observed for CoCrMo – Ti6Al4V couples at the displacements studied. Prior to the start of fretting, a gradual ennoblement of the OCP was observed. At the start of fretting a cathodic shift in OCP was observed. The magnitude of the maximum cathodic shift in OCP was dependent on the fretting amplitude applied to the interfaces (Fig 4b). For δ_a = 10 and 25 µm, the OCP was seen to gradually increase with time during the application of fretting. After fretting, the OCP was monitored for a further 1000 seconds. In the case of δ_a = 10 and 25 µm, the OCP was similar to initial values of OCP observed (~ -0.1 V). For tribo-couples slid at δ_a = 50 and 150 µm, a sudden decrease in OCP was observed at the onset of fretting indicating abrasion and depassivation of the metallic

surfaces. The cathodic shift in OCP was sustained and seen to further decrease over the duration of the test until fretting was stopped. OCP was seen to enoble after fretting was ceased although did not recover to values observed at the start of the test (- 0.27 to -0.30 V); indicative of the enhanced localised corrosion at the interface.
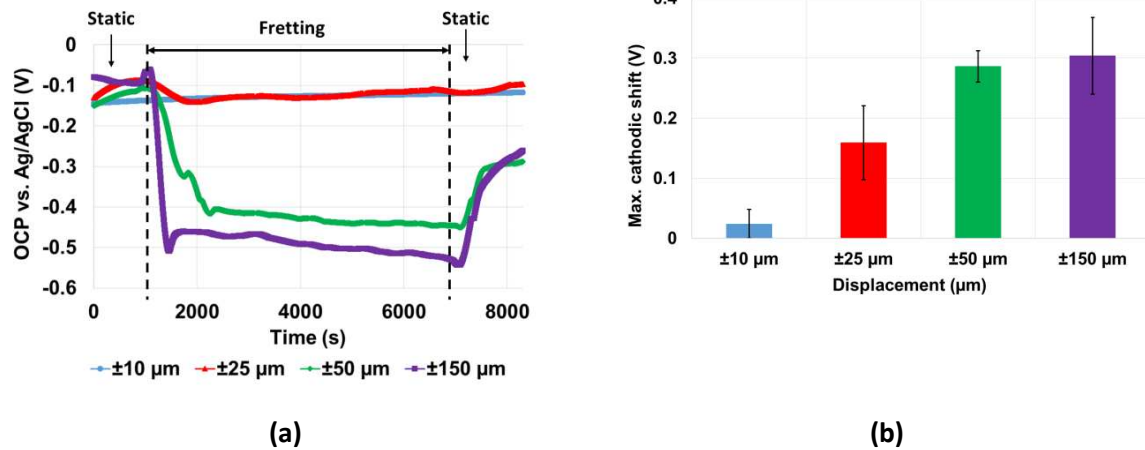

(a)   **(b)**

Fig 4 – a) Evolution of OCP and b) maximum cathodic shift in OCP at the displacement amplitudes studied (results show mean ± standard error).

3.2. Fretting-loops and Energy Dissipation

Fig 5 shows the tangential force (F_t) vs displacement (δ) and evolution of cumulative dissipated energy (E_d) as a function of number of cycles for the CoCrMo-Ti6Al4V couple subjected to fretting-corrosion. Upon initiation of fretting displacements at δ_a = ±10 µm and ±25 µm, a stick regime was observed with an increase in F_t being observed at δ_a = ±25 µm when compared to δ_a = ±10 µm (Fig 5a). The cumulative amount of energy dissipated at the contact for both δ_d = ±10 µm and ±25 µm is also shown. A linear increase in the cumulative dissipated energy was observed for both displacements corresponding to and energy dissipation rate of 30 µJ/cycle and 113 µJ/cycle at δ_d = ±10 µm and ±25 µm, respectively. A sliding to displacement ratio of $\frac{\delta_S}{\delta_d}$ = 0.029±0.002 and 0.068±0.004 was observed for contacts subjected to δ_d = ±10 µm and ±25 µm respectively. This is firmly in the stick regime as identified by Fouvry et al [37] and was seen to remain in the stick regime for the duration of the test.

Fig 5b shows the different fretting loops observed at points during the test of a CoCrMo – Ti6Al4V contact subjected to δ_d = ±50 µm. A 'mixed' fretting regime characterised by the transient nature of slip at the interface was observed. A partial-slip regime was observed in the first ~ 600 cycles of fretting transitioning into a gross slip regime for the remainder of the test. A representation of the partial-slip fretting loop is shown at the 500th cycle. A period was observed at the 550th cycle whereby the partial-slip regime accommodated a higher degree of 'actual interfacial slip' prior to transition into the full

gross slip regime. The transition to gross slip was accompanied with a significant reduction of the tangential force as depicted by the fretting loop obtained at the 6000th cycle. The graph of cumulative energy is also shown in Fig 5b. The rate of cumulative energy dissipation as a function of cycles differs for the two regimes. A transition in the rate of change of dissipated energy was observed at approximately 600 cycles from 1120 µJ/cycle to 3820 µJ/cycle. This correlates with the observations made above. The energy dissipated per cycle at the gross slip regime was more than three times greater when compared to the partial-slip regime. Interestingly, a decrease in tangential force was observed in the gross-slip regime indicating that energy dissipation in the gross slip regime is slip dominated. The transition in the fretting regime at δ_d = ±50 µm was further confirmed by the slip ratio criteria. Below 500 cycles, $\frac{\delta_s}{\delta_d}$ = 0.21 ± 0.11 indicating a partial-slip regime. After 550 cycles, $\frac{\delta_s}{\delta_d}$ = 0.634±0.114 indicating transition into the gross-slip regime.

Fig 5c shows the fretting regime at δ_d = ±150 µm. A gross slip regime was observed throughout the duration of the test. The cumulative dissipated energy graph (Fig 5c) shows constant energy dissipation per cycle throughout the duration of the test. An energy dissipation rate of 19060 µJ/cycle was observed when δ_d = ±150 µm. The sliding – displacement ratio was seen to remain stable throughout the tests, $\frac{\delta_s}{\delta_d}$ = 0.85 ± 0.01 indicating a gross-slip regime.

(a)

(b)

(c)
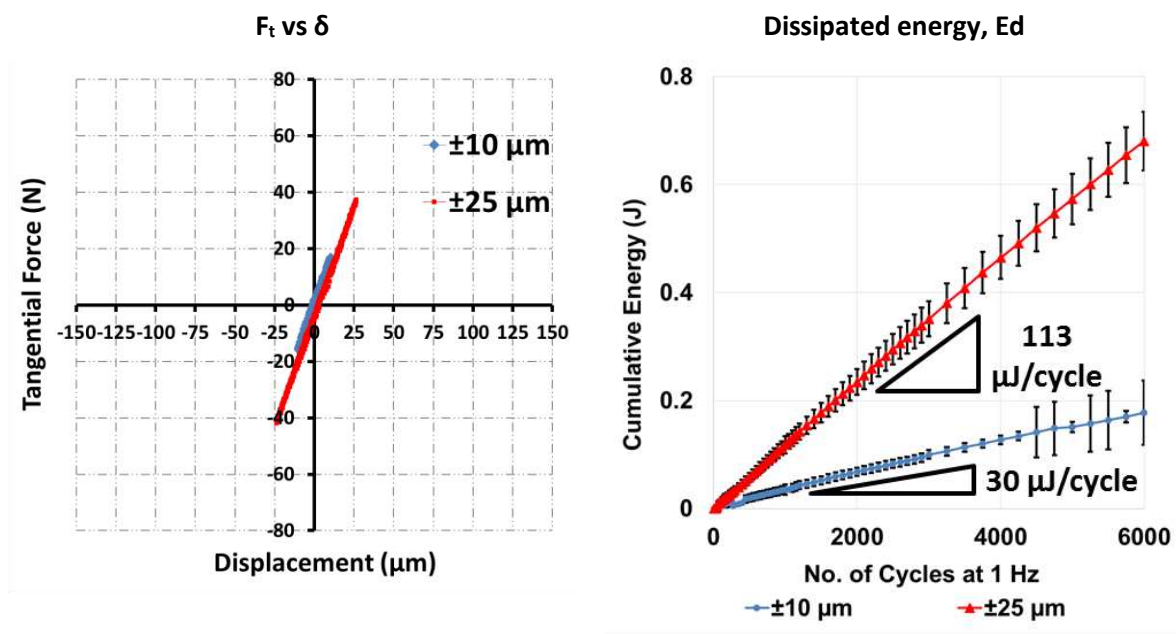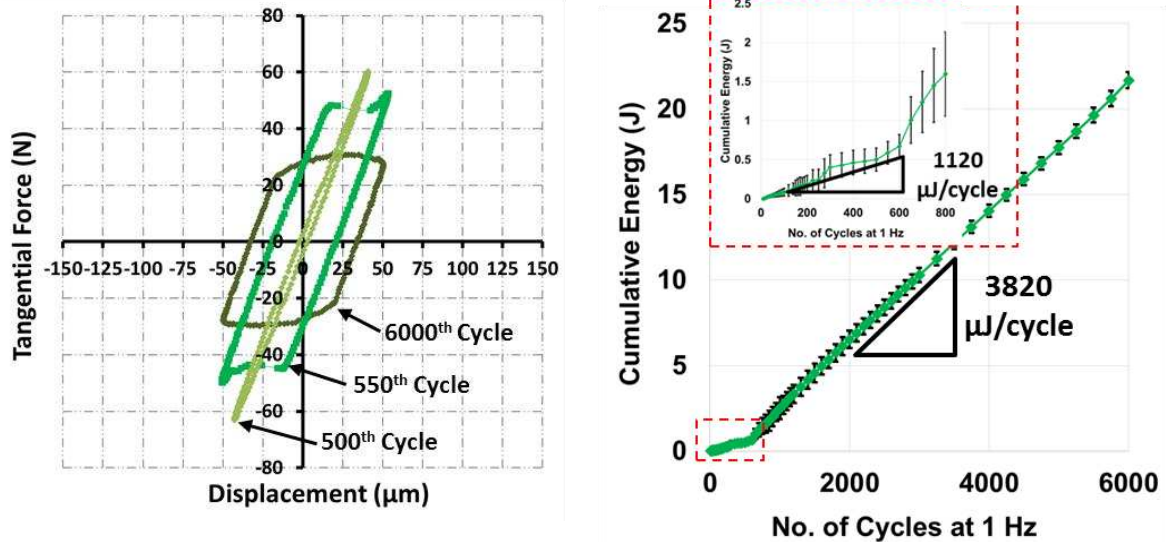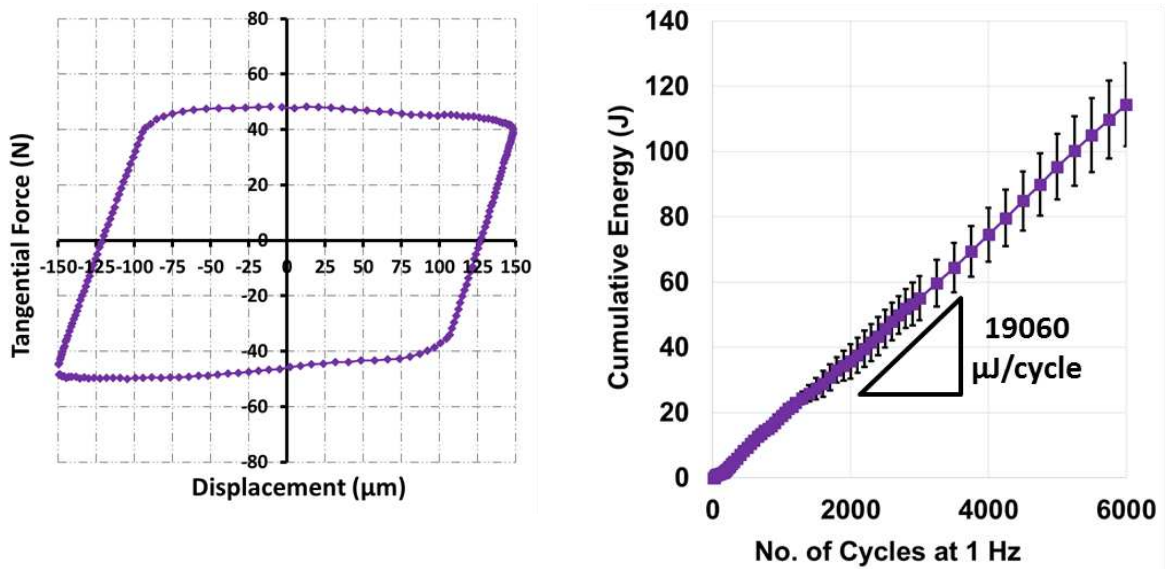
Fig 5 – F_t vs δ and cumulative dissipated energy vs number of cycle for CoCrMo-Ti6Al4V couples at a) 10, 25 b) 50 and c) 150 μm

3.3. Surface Topography and Material Loss

The 3D and 2D surface profiles of the CoCrMo – Ti6Al4V combination are shown in Fig 6a and 6b, respectively. At $δ_a = ± 10$ μm, no visible signs of material loss on the CoCrMo ball or Ti6Al4V flat could be observed. At $δ_a = ± 25$ μm, a thin annulus at the edges of the contact area on the CoCrMo ball showed evidence of materials loss. The maximum material loss within the annulus was ~ 300 nm. Across the entire central partial-stick region, third-body materials generated from the contacting interface was observed. The Ti6Al4V flat showed no evidence of material loss although some material transfer was observed. At $δ_a = ± 50$ μm, both surfaces showed evidence of material loss and

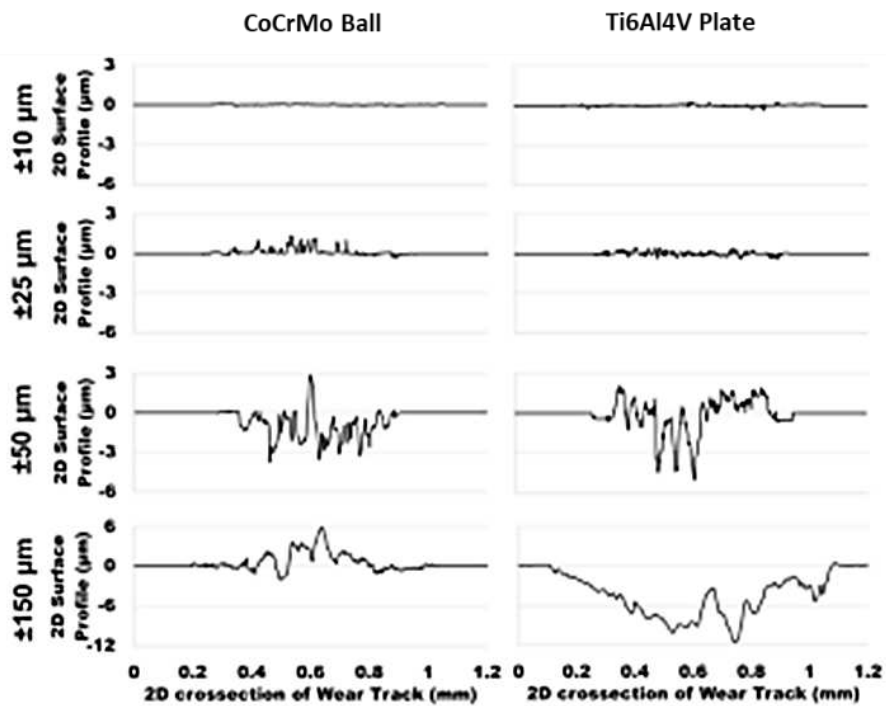redistribution of material within the contact area. Clear directionality in the resultant surface topography was observed. Both surfaces demonstrated evidence of positive volume with a thickness up to 3 μm with reference to the original surface. At δ_a = ±150 μm mass loss from both surfaces was observed. The Ti6Al4V surface was mainly characterised with larger wear depths (maximum depth ~11 μm) with no evidence of material build-up within the degraded area. Similar observations were made for the CoCrMo surfaces, although with some localisation of material build-up in the contact area. In general, the size of the wear contact surface for both ball and flat components at δ_a = 10 – 25 μm was similar to the initial Hertzian contact width (2a = 500 μm).

Fig 6c and 6d show the volumetric material loss (i.e. material below the datum) and material build-up (i.e. material above the datum) for the CoCrMo ball and Ti6Al4V plate, respectively. No measurable volume loss could be determined on the CoCrMo ball (Fig 6c) at δ_a = 10 μm and any surface deviations observed were in the order of the original surface roughness. An increase in material loss was seen with increasing displacement amplitudes from δ_a = 25 - 50 μm, with no further increase in volume losses at δ_a = 150 μm when compared to δ_a = 50 μm. Material build-up on the CoCrMo ball (Fig 6c) was seen to vary correlate with increasing displacement.

Fig 6d shows the volumetric material losses and build-up for the Ti6Al4V plate. No measurable volume loss could be determined on the Ti6Al4V plate at δ_a = 10 μm and any surface deviations observed were in the order of the original surface roughness. From δ_a = 25 - 150 μm, an increase in volume loss was observed with increasing displacement amplitude. Material build-up was seen to increase from δ_a = 25 – 50 μm little changes in material build-up were observed at δ_a = 150 μm when compared to the lower displacement amplitudes.

CoCrMo Ball　　　　　　　　**Ti6Al4V Flat**

±10 μm

±25 μm

±50 μm

±150 μm

(a)

CoCrMo Ball　　　　　　　　**Ti6Al4V Plate**

±10 μm

±25 μm

±50 μm

±150 μm

2D crossection of Wear Track (mm)　　　2D crossection of Wear Track (mm)
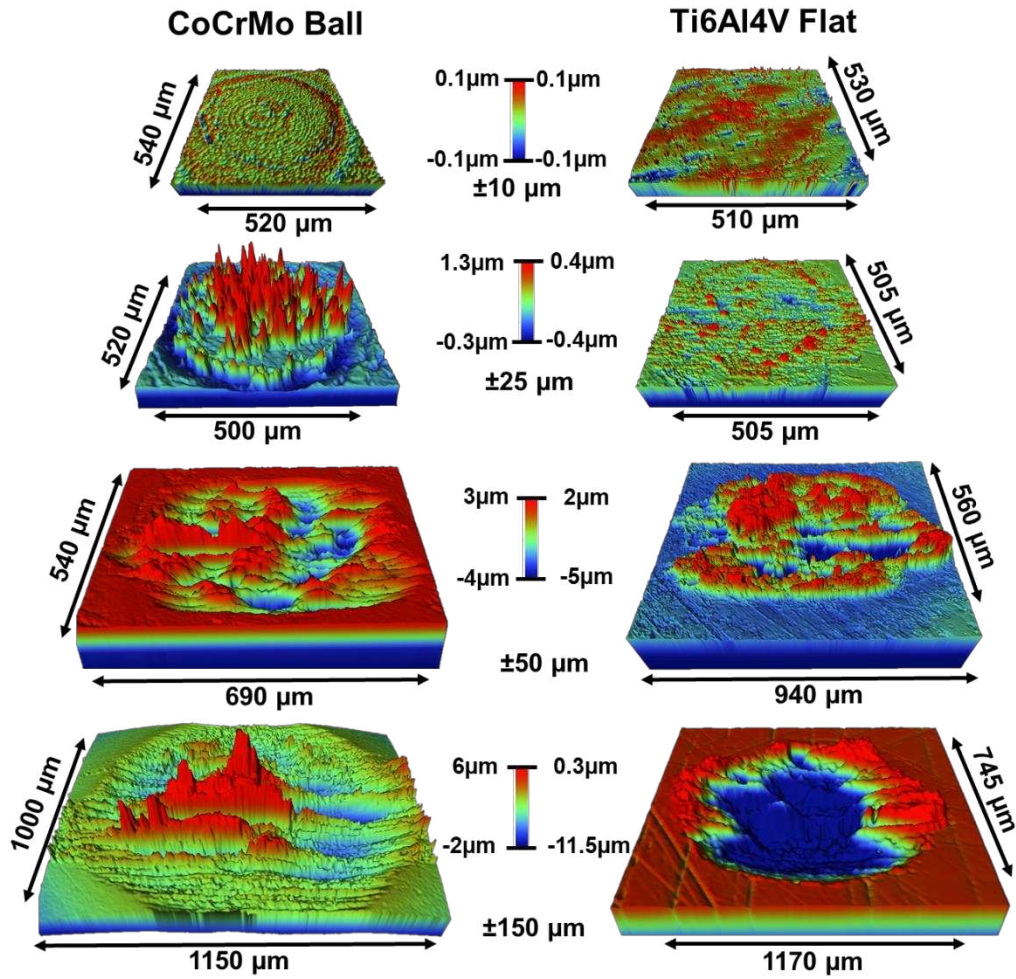
(b)
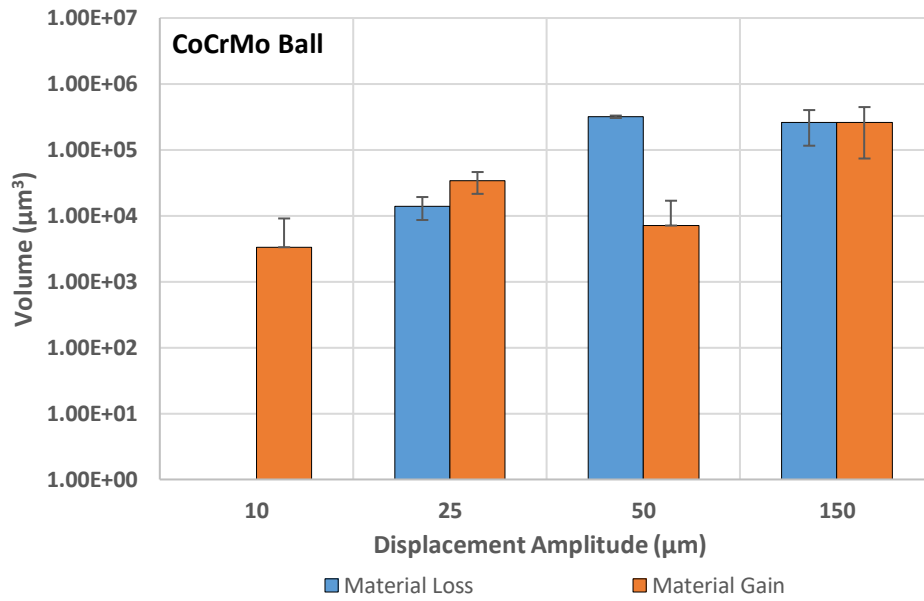
(c)
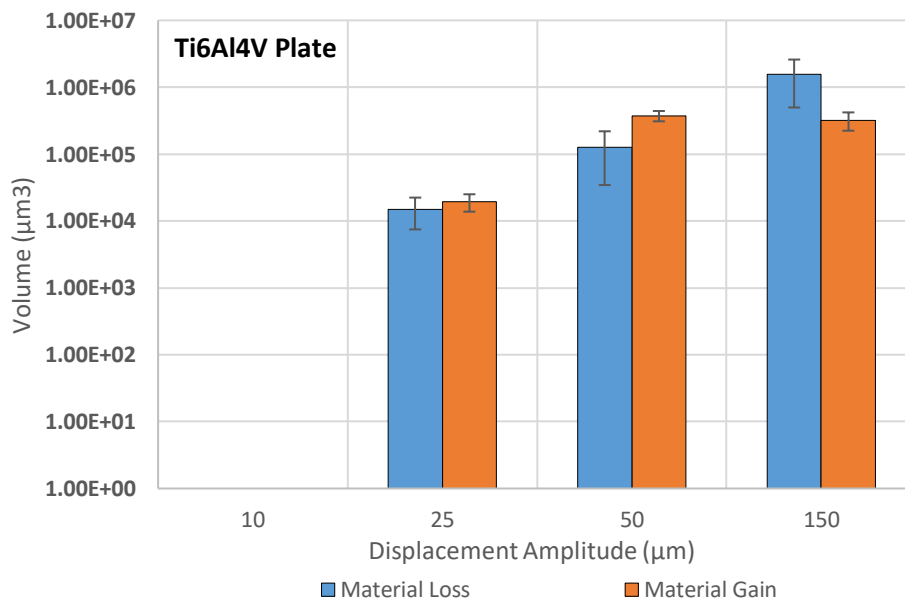
(d)

Fig 6 – a) 3D and b) 2D surface profiles of CoCrMo and Ti6Al4V areas after fretting-corrosion measured using VSI. Fig 6c and 6d show the material volume loss and material gain on each surface. Note the y-axis on Figs 6c and d are on a logarithmic scale. Volume losses were not measurable at δ_a = ±10 µm

3.4. Transmission electron microscopy

Fig 7 shows the bright and dark-field TEM micrographs obtained from the Ti6Al4V disc after fretting corrosion. Fig 6a shows a TEM micrograph of the polished Ti6Al4V alloy in the absence of fretting and corrosion. A naturally occurring thin protective oxide layer typically known as the "passive layer" was

visible from the bright-field image. Evidence of a nano-crystalline microstructure was observed within top 150 – 200 nm of the alloy surface, directly beneath the passive layer. The red dashed-line in Fig 7a is drawn to distinguish the nano-crystalline structure above from the single-crystal structure beneath it. The single-crystal structure beneath is identifiable by its larger grain size relative to the smaller grain-sizes above the red dashed-line, identifiable using dark-field imaging. The bright and dark-field micrographs of Ti6Al4V after fretting at ±10 μm are shown in Fig 6b. When compared to Fig 7a, evidence of strain-induced re-orientation of the subsurface was observed. A similar, but more profound pattern was observed at δ_d = ±25 μm (Fig 7c).

Fig 7d shows the bright and dark-field micrographs of the Ti6Al4V subsurface when subjected to fretting-corrosion at δ_d = ±50 μm. When compared to lower displacements, significant changes in the sub/surface chemistry and crystallinity were observed. Directly beneath the two layers of protective Pt, a 2-3 μm thick 'mechanically mixed' layer was observed. This consisted of a fine nano-crystalline structure consisting of particulates and amorphous materials. Three distinct regions of this material was observed across the interface (boundary's highlighted in orange). Evidence of a poly-crystalline Ti6Al4V microstructure was seen directly beneath the surface layer with a grain size similar to the reference surface. Material transitioning into the layer from the bulk Ti-alloy can be seen.
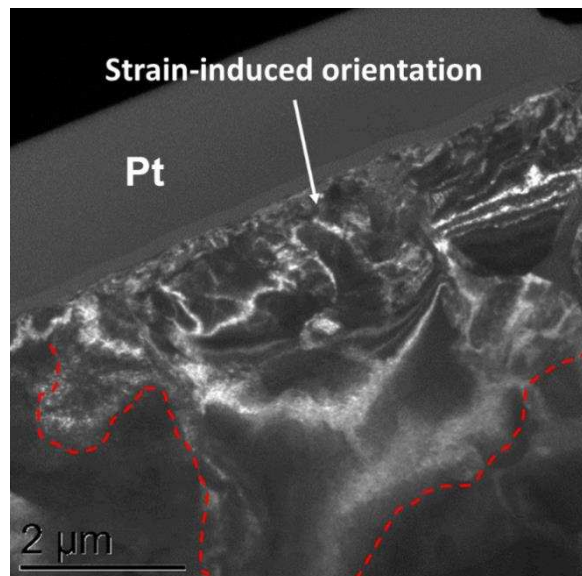
From the micrographs shown in Fig 7e (δ_d = ± 150 μm), subsurface strain-induced refinement of the Ti6Al4V microstructure was observed when compared to the reference samples. Evidence of cracking and mixing of organic species at and within the interface was visible.

Bright feild	Dark field
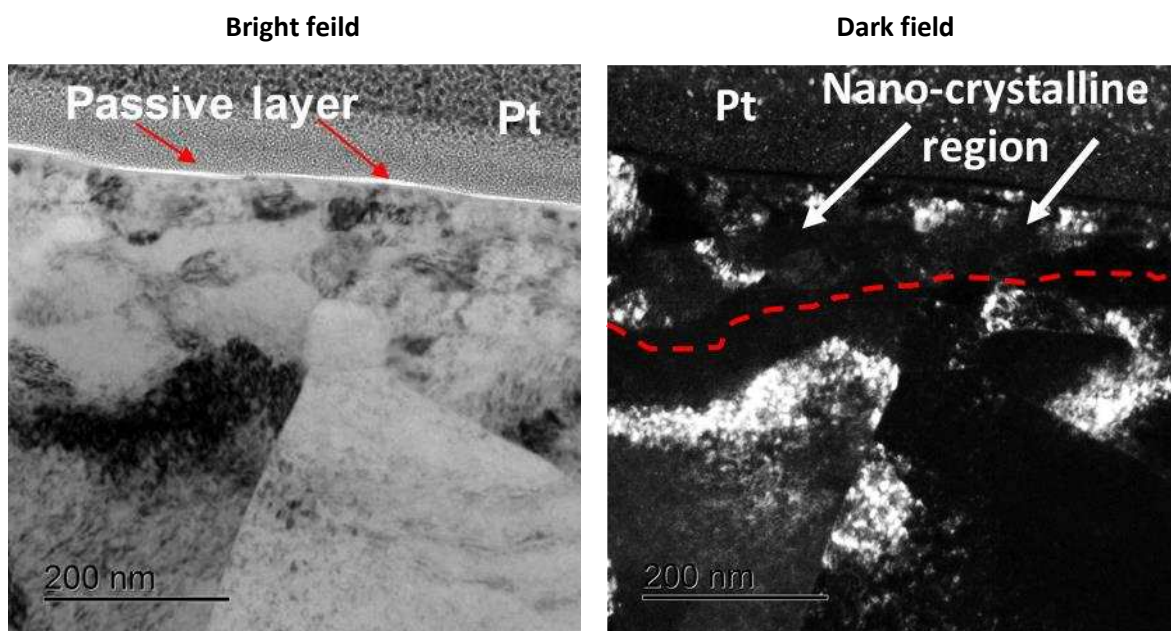
(a)
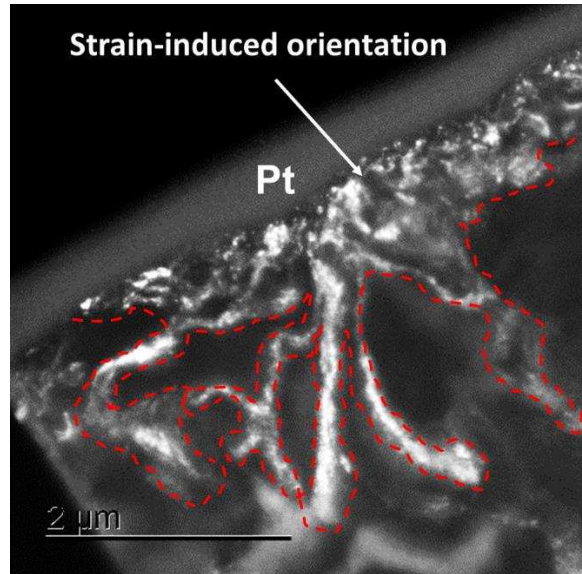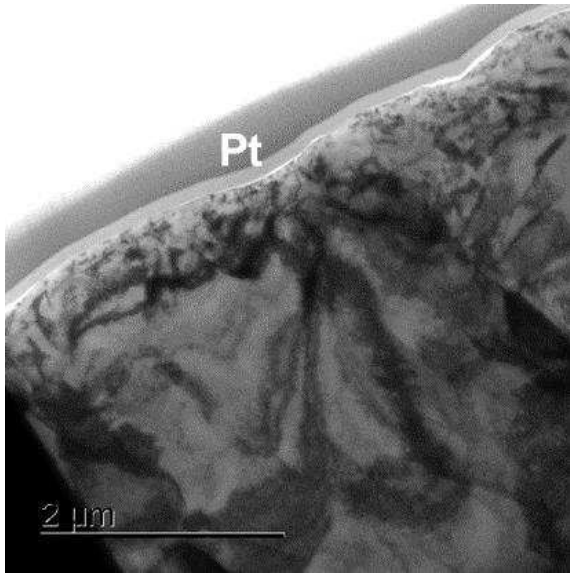
(b)
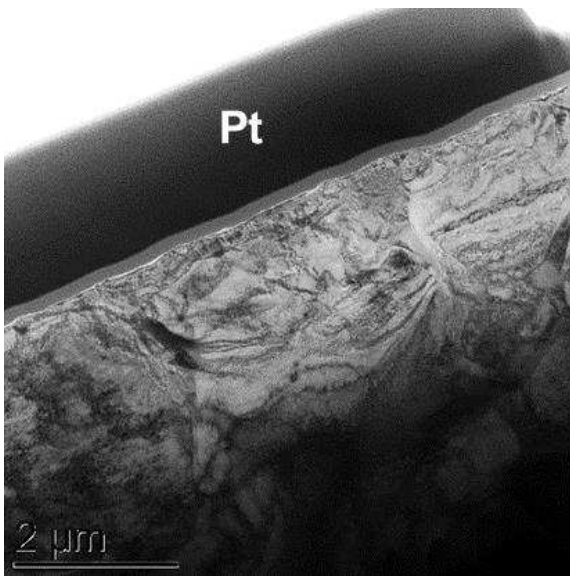
(c)
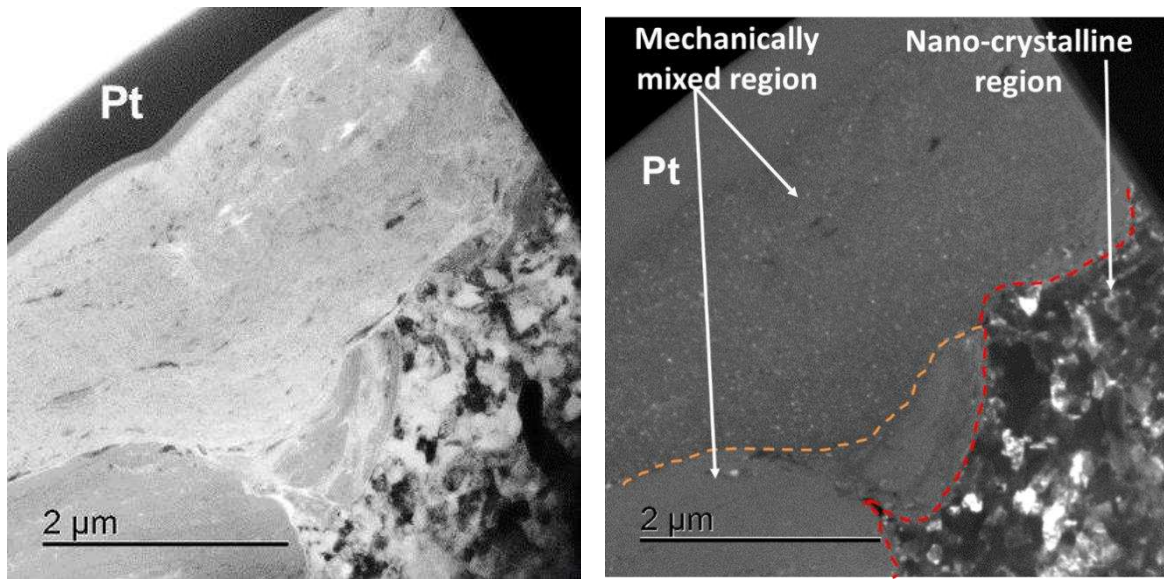
(d)
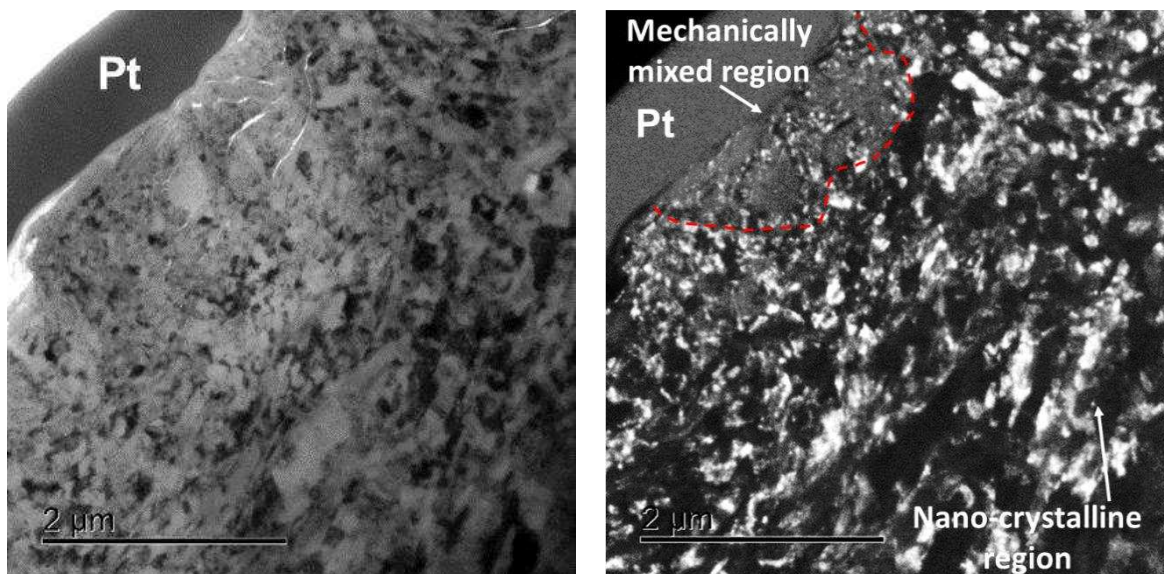
(e)

Fig 7 – Sub-surface bright-field and dark-field TEM images for a) Reference polished Ti6Al4V surface and after being subjected to fretting-corrosion at b) 10 c) 25 d) 50 and e) 150 µm.

Fig 8 shows the EDX and SAED analysis to further characterise the three different structures observed on Ti6Al4V surfaces subjected to δ_a = 50 µm (Fig 7d). Three different structures were seen; the fine particulate, mechanically mixed structure is denoted 'A'. The non-particulate structure directly beneath structure A is denoted 'B' and the nano-crystalline structure beneath both structures 'A' and 'B' is denoted 'C'. SAED confirms the structure 'A' to be nano-crystalline. Area 'B' appears to be amorphous as evidenced with the shroud of bright spots forming a ringed pattern. Structure 'C' is confirmed to be nano-crystalline Ti6Al4V material. EDX mapping of the cross-section shows that structure 'A' is a material rich in Co, Cr, Ti, Mo, V, Al, C O and Cl suggesting the material is complex

mixture of tribo-chemically mixed materials originating from the CoCrMo, Ti6Al4V and lubricant. The map also shows evidence of localisation of Ti within the mechanically mixed products of structure 'A' which may be indicative of Ti rich particulates. For structures 'B' and 'C', EDX mapping identifies the chemical constituents of both structures to have originated from the Ti6Al4V alloy. Evidence of O and Cl in amorphous structure of 'B' was observed. The combination of SAED and EDX mapping confirms structure 'C' to be a bulk Ti6Al4V material.
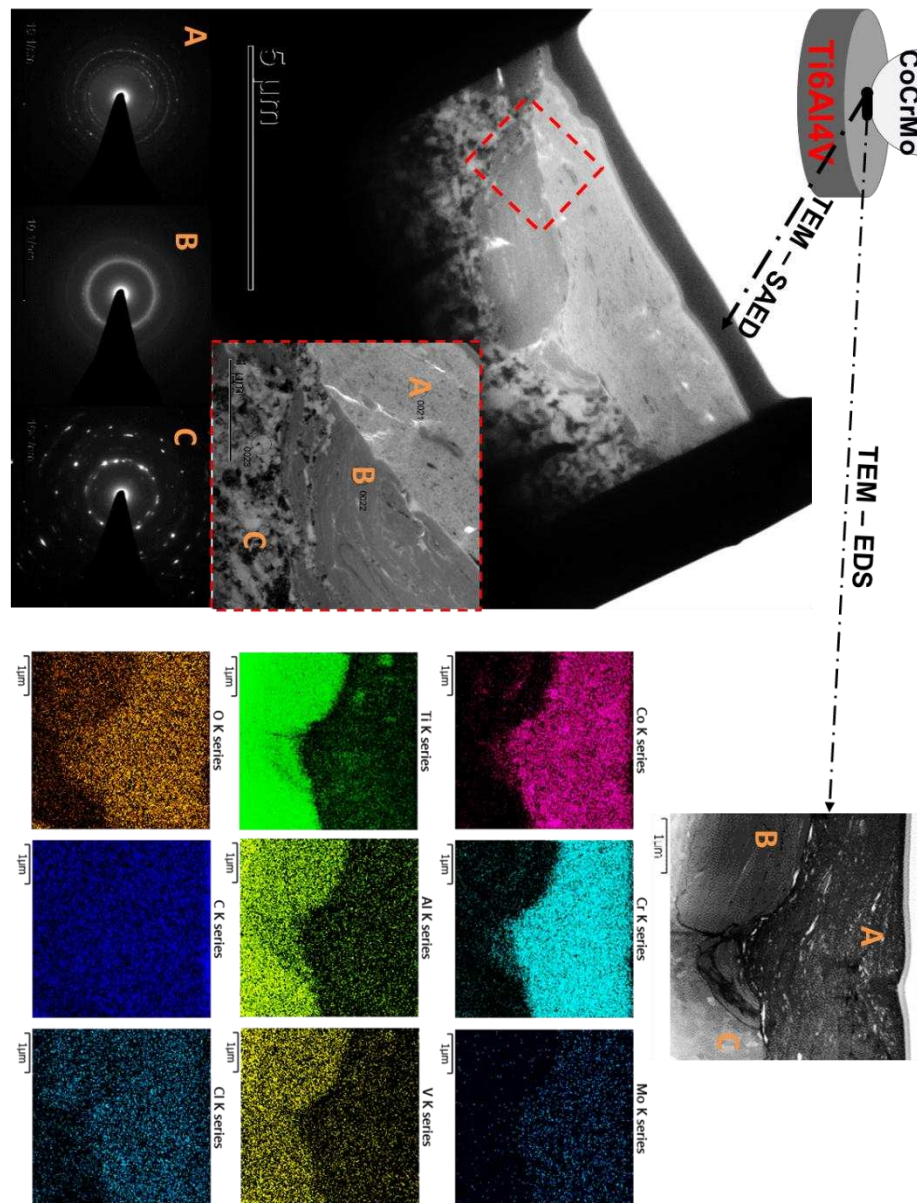
Fig 8 – Bright-field, EDX and SAED analysis of the three different structures observed on Ti6Al4V surfaces subjected to δ_a = 50 μm.

3.5. Nano-mechanical evaluation

Nano-indentation was performed on cross-sections of the Ti6Al4V prior to and after simulated fretting corrosion (Fig 9a). Figs 10b and 10c show the obtained force displacement data for bulk Ti6Al4V and interfacial layer the when indented between ~ 20 – 60 nm, respectively. An increase in hardness (Fig 9d) and Reduced Modulus (E_r, Fig 9e) was observed for the tests subjected to fretting-corrosion when compared to the Ti6Al4V surface.
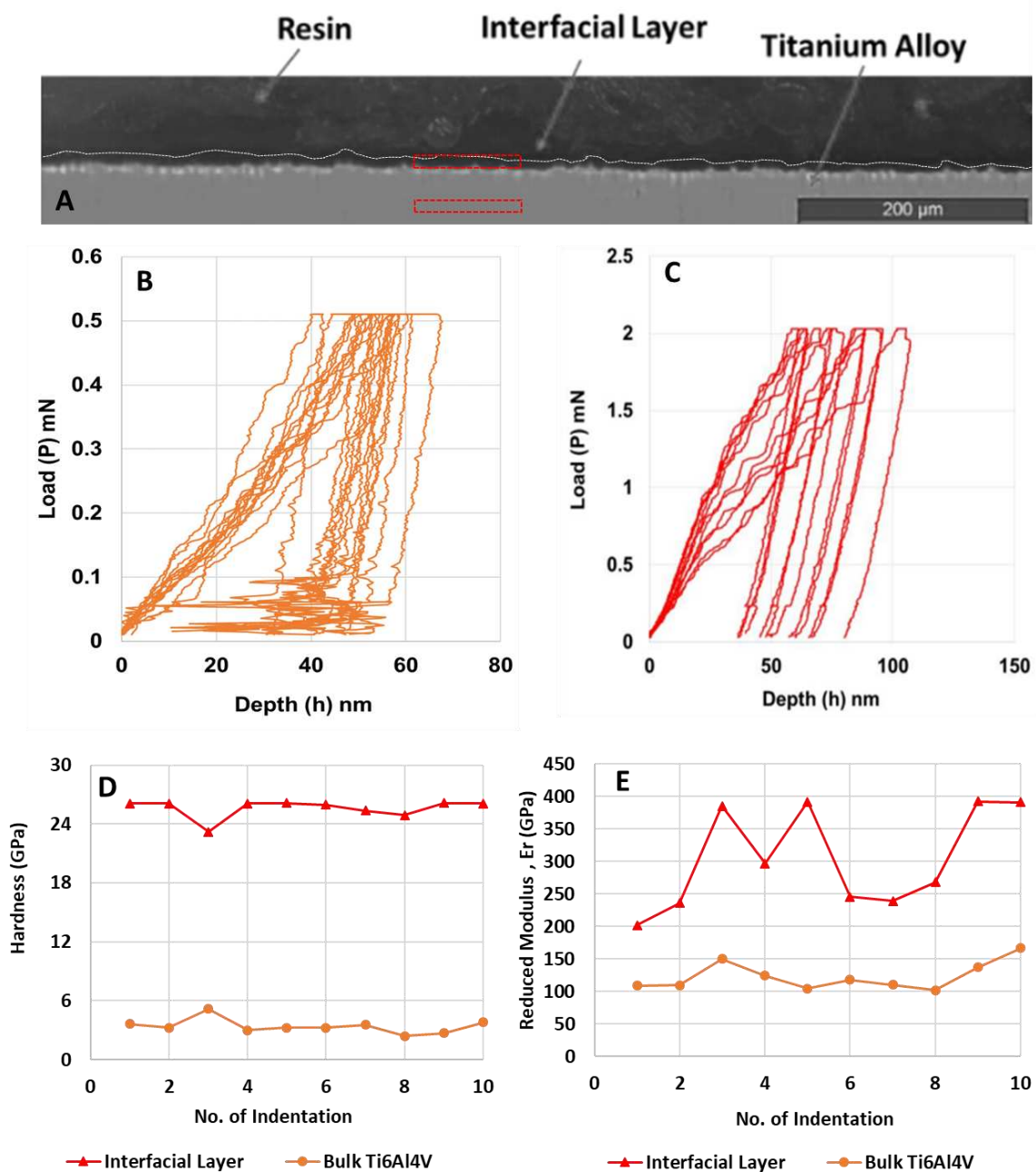
Fig 9 – a) cross-sectional optical microscope image showing the interfacial layer (white dashed) and the region where nano-indentation was made on the interfacial layer and bulk Ti6Al4V (red dashed). Fig 9b and c show the raw force-displacement obtained. Fig 9d and e show the hardness and Reduced Modulus data determined using the Oliver and Parr approach.

4. Discussion

The aim of this study was to investigate the role of interfacial slip mechanisms on the evolution of subsurface microstructure and the nature of the tribo-products formed as a result of fretting-corrosion in simulated biological environments. A combination of methods have been used to demonstrate the roles of energy dissipation at the contact on the de-passivation processes via measurement of OCP, evolution of subsurface micro-structure and the physio-chemical nature of tribo-products generated at the interface. This study has shown that CoCrMo-Ti6Al4V fretting interfaces are highly complex and transient. Subtle changes in slip regime were seen to influence the material loss mechanisms, electrochemical processes and sub-surface microstructure. The complexity of the interfacial system has been shown through a series of simple, but controlled, fretting-corrosion tests. The use of site specific TEM-EDS for the analysis of fretting-corrosion contacts has further demonstrated that the nature of the tribo-material formed in the fretting contact is significantly different when compared to CoCrMo sliding orthopaedic systems. Strain induced transformation of the CoCrMo FCC phase to HCP has been noted to occur up to ~ 100 nm in the subsurface along with the formation of carbonaceous tribofilms on the surface seen for sliding systems [30].

The mechanisms of subsurface microstructural changes in biomedical fretting-corrosion contacts have not been studied in great detail. Material build-up within a Ti6Al4V-CoCrMo fretting-corrosion contacts is not a simple formation of abraded oxides on a surface as suggested in previous literature. In fact, it is a complex and dynamic mechano-chemical mixing process where no discreet interface between damaged and undamaged material is observable. These processes result in the formation of materials with very different mechanical and chemical properties when compared to the initial surfaces, penetrating the apparent surface > 1 μm in some cases. The observations made in this study go further towards understanding the degradation processes occurring at fretting-corrosion interfaces *in vivo* for orthopaedic applications such as hip/knee modular-taper connections, fracture fixation plates, spinal facet joint instrumentation.

4.1. The links between fretting-corrosion and subsurface microstructure.

The frictional forces arising for the shearing of two contacting surfaces can be better conceptualised as an energy dissipative processes whereby different pathways for dissipation exist. This is particularly the case for fretting contacts where gross sliding of the contact may not have fully developed. The seminal work of Mindlin, Vingsbo and Soderberg [31] and Fouvry et al [27] consider this in a purely mechanical context. The links between wear (i.e. in this case purely a physical process) and dissipated energy have been clearly shown in the literature for fretting contacts [10, 28, 32-34]. Similarly, the links to corrosion and its synergies during tribocorrosion have been quantified in recent work for

fretting-corrosion contacts in simulated biological environments [35-37]. However, a full consideration and description of the degradation processes occurring at interfaces and the links with energy dissipation processes are still relatively unknown. This work shows the importance of considering corrosion aspects in the degradation and energy dissipation processes of contacting biomaterials; although not directly quantified in this study. Fig 10a shows the correlation of between total dissipated energy (E_d) and total volume loss (V_{Lt}) and total volume gain (V_{Gt}) for tests conducted according to Eq 1 & 2. With increasing total dissipated energy, achieved via incremental increases in displacement amplitude, an increase in the material losses / gains was observed. This correlates with existing literature mentioned previously. Fig 10a and 10b further breaks the contribution to mass loss down further presenting total volume losses or gains for each material as a percentage of overall mass loss/gain. Volume losses (Fig 10b) from the CoCrMo surfaces were seen to account for ~ 50 to 70% of the overall volume losses at δ_a = 25 and 50 μm, respectively. Volume loss of the Ti6Al4V was seen to dominate at δ_a = 150 μm. This is complimented by Fig 10c, which shows how the build-up of material within the contact in the Ti-alloy plate increases from δ_a = 10 to 50 μm. These observations can be explained by the nature of slip and energy dissipation pathway occurring at the interface. At 10 – 50 μm a partial slip regime is established with varying degrees of energy dissipation taking place at the interface. It is conceivable that any debris that is generated within the contact within these regimes will be retained to some degree within the contact, contributing to the enveloping degradation processes. At δ_a = 150 μm, the contact is experiencing a gross-slip regime where the sliding area is greater than the nominal contact area resulting in ejection of debris form the interface. This is in line with the recent findings from Clark et al [37] who demonstrated the nature of the debris released from fretting-corrosion contacts correlated within the slip processes occurring at the interface.

The detailed TEM analysis conducted in this study enabled us to understand these dissipation pathways. Within the stick regime at δ_a = 10 and 25 μm, a low energy dissipation rate is observed when compared to the larger displacement amplitudes. Whilst there is little evidence of depassivation of the surfaces and no measurable material loss, TEM analysis indicates that changes in the sub-surface microstructure occurs. The degree of these changes appear to increase with increasing displacement amplitude and energy dissipation. This demonstrates that in the absence of no considerable slip, low wear and little evidence of depassivation of the metallic surfaces, dissipative processes at the interface are implicated in the sub-surface microstructural changes. This suggest that under conditions where low levels slip, cyclic shear stress at the interface will manifest itself in dislocation motion and the formation of high density dislocation structures resulting in irreversible plastic deformation of the subsurface; characteristic of a fatigue based process. In fact such alterations

in subsurface microstructure have been observed in other biomaterials subjected to cyclic stresses, in the absence of tribological contact [38].

As the nature of slip changes it is evident that the dissipative pathways change. At δ_a = 50 μm, the fretting contact exhibits a partial slip, transient regime exists where energy is dissipated through wear and corrosion (indicated via OCP measurement), subsurface microstructural changes and tribochemical processes. This is further complicated by the elastic-plastic nature of the deformation within the fretting contact. TEM analysis shows that the nature of the interface changes significantly when compared to the control surface and tests conducted at δ_a = 10 and 25 μm. Refinement of the subsurface microstructure, the formation of localised areas of amorphous materials consisting of materials derived from the Ti-alloy and lubricant and the formation of a relatively thick nano-crystalline materials consisting of metal oxides and organic matter was confirmed by EDS and SAED analysis. The formation of these materials within the contact may explain the transient nature of the contact due to the gradual build-up and subsequent fracture of the interface layers, as evidenced in Fig 8. It also gives further insight into the observations made by Swaminathan who suggested that CoCrMo may dominate the outcomes for mixed-metal fretting-corrosion contacts. With the generation and retention of such layers within the contact, the nature of the interface that facilitates slip is significantly different compared to the original nascent surfaces. TEM-EDS analysis shows the interface is a complex mixture of mixed metal oxides, dominated by Co and Cr which provides further insight into the observations made by Swaminathan [35]. At δ_a = 150 μm and based on the initial predicted Hertzian and final nominal contact width measured by VSI, the contact is likely incipient sliding. It is evident that subsurface microstructural refinement occurs when compared to the control sample. The nature of the interface is also very different compared to the fretting-corrosion contacts slid at lower displacement amplitude. No evidence of the formation and retention of oxides within the contact was observed and it is likely that any debris generated is likely ejected from the contact. Evidence of subsurface cracking and mechanical mixing of the Ti-alloy was seen suggesting fatigue is a component of the degradation mechanisms, although at δ_a = 150 μm wear will likely dominate.
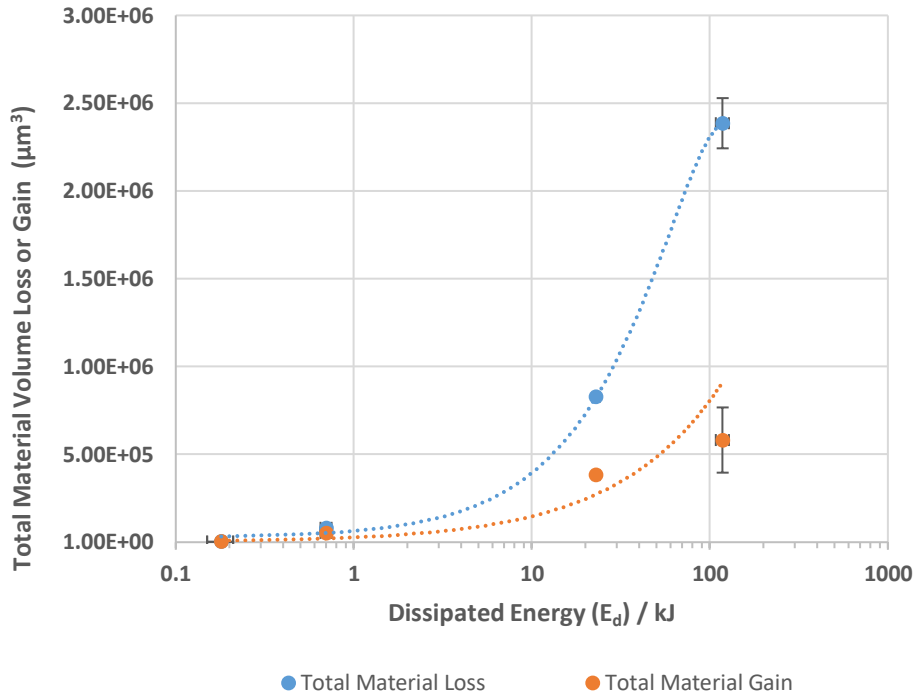
(a)
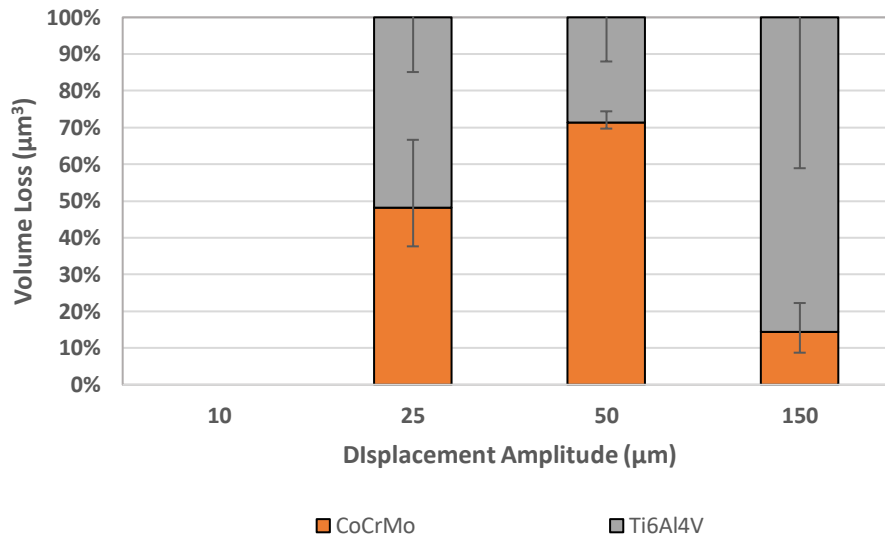
(b)
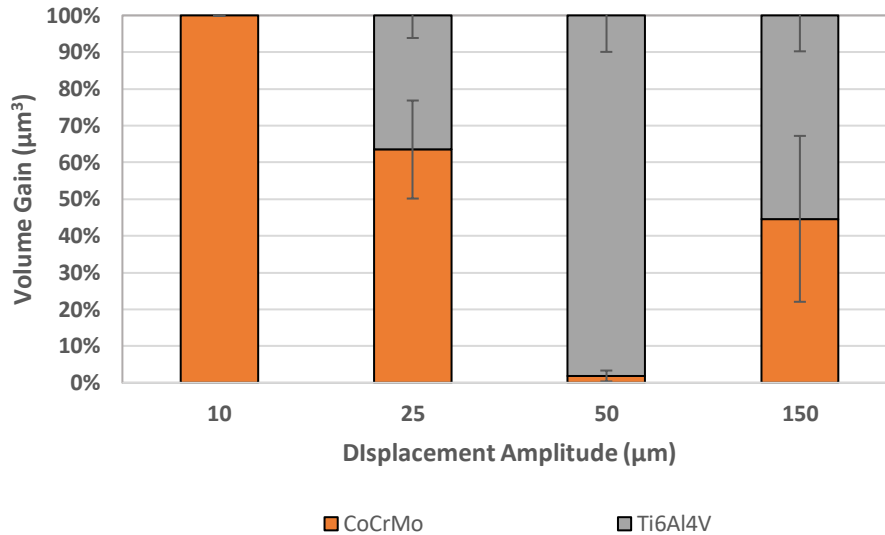
(c)

Fig 10 – a) Correlation of volume losses / gains with dissipated energy and percentage contribution of b) material loss or c) material gain from CoCrMo and Ti6Al4V surfaces.

4.2. What does this mean for in-vivo applications?

Fretting-crevice corrosion or mechanically assisted crevice corrosion has been of interest for a number of years due to the biological implications of tribocorrosion debris within the biological environment. A wealth of in-vitro and retrieval analysis exists characterising the fretting-corrosion response, evolution of surfaces topography and debris release. The presence of complexed metal oxides at the interface, as shown in this study, is widely reported in both in vitro and retrieval literature and often used a criteria for grading corroded metallic implants. Despite this, the formation mechanisms and their subsequent implications on degradation are not well understood. The preferential degradation of the harder CoCrMo alloy relative to the softer Ti-alloys has been highlighted in retrieval analysis [23], yet no robust mechanism of such has been proposed. To date the degradation mechanisms occurring at the fretting interface have mainly been considered as a surface processes with little attention paid to the dynamic microstructural and tribochemical changes. Moharrami et al [19] hypothesized that in-vivo oxidation of the surface (i.e. formation of thicker oxide layer on the surface) could have a significant effect on the surface mechanical properties of the Ti alloy causing it to become harder and having a higher tendency to abrade the CoCrMo surface, albeit examined in static corrosive conditions.

TEM data presented in this study shows the nature of the fretting-interface is not discrete and varies substantially compared to the original contacting surfaces. The formation of thick and hard mixed metal-oxide layers, refinement and mechanical mixing of the Ti-alloy sub-surface has been observed

depending on the nature of slip at the interface. This raises additional questions as to what is actually measured during routine gravimetric or volume analysis measured using surface scanning techniques. Data here shows that despite a measurable wear loss, changes to subsurface volumes and redistribution of material at the interface is significant. The in-vitro observations made in this study correlate well with the *in vivo* analysis presented in [24] where location specific subsurface refinement and microstructural al changes were observed in Ti-alloy bi-modular components. Sauger et al [39] showed that nano-crystalline structures do form in Ti6Al4V under dry fretting conditions, and are located within highly plastic regions beneath the layers of already worn products. The structure was called 'tribologically transformed structures' (TTS) in their study and further characterisation of the structure showed that the TTS can be more than two times harder than the original bulk Ti6Al4V alloy [39]. In this study, the increase in hardness and reduced modulus is due to the presence of tribo-material formed within the contact. The refinement of the subsurface microstructure due to mechanical shear and the resultant mechanical mixing of oxidised material will lead to a surface with altered material mechanical properties when compared to the bulk materials. It is anticipated the hard interfacial fretting-induced materials, as observed in this study, would largely influence the wear and corrosion phenomena at the interface. From the transition to gross slip, the softer Ti6Al4V is no longer in contact with the CoCrMo counter-body. Rather, the CoCrMo is in direct fretting contact with the interfacial layer several times harder than itself, thus it is expected that CoCrMo would suffer more wear in such condition whilst Ti6Al4V would experience no wear. If such hard phases form in-vivo, it proposes a more plausible reason than those given by Moharrami et al [19] as to why CoCrMo wears more than its softer Ti6Al4V counter-part.

The study presented has its limitations. The manifestation of fretting-corrosion or MACC in-vivo has been shown through retrievals to include corrosion damage mechanisms such as inter-granular and pitting corrosion, oxide induced stress corrosion cracking (OISCC) [8, 20]. While it is known that these mechanisms can be sustained beyond the cessation of mechanical action, an initial mechanical action is required to create the crevice conditions for corrosion dominated mechanisms to manifest. The authors appreciate this, however this study was aimed to address the less understood aspect of fretting-corrosion which is concerned with the significant changes to both the surface and the subsurface of CoCrMo and Ti6Al4V alloy as evidenced in retrieval studies [24]. The in-vitro tests carried out in this study were short-term, lasting 6000 cycles. This study has therefore only provided insight into the early-stage damage mechanisms with some indications of possible long-term failure mechanisms.

5. Conclusions

In the present study, fretting-induced subsurface refinement and microstructural al changes of the microstructure and tribo-chemical reactions occurring on Ti6Al4V alloy surfaces was characterised at all three fretting regimes including the mixed regime. The degree of subsurface microstructural refinement was observed to be energy dependent while the manifestation of the energy dissipation was dependent on the contact condition, that is, the fretting regimes. The key findings of this study can be summarised as:

1. The type of slip at the fretting-corrosion interface affects the degree and type of degradation product at the interface. Debris was seen to be retained within the contact under 'mixed' fretting regimes.

2. Complex subsurface microstructural and mechanical mixing processes were observed where an increase in nano-hardness was observed. After fretting, where slip had occurred, a discrete Ti-alloy interface was no longer present.

3. It is hypothesised that the more severe degradation of CoCrMo surfaces with respect to Ti-alloy is driven by the formation of the hard mixed metal oxides arising from the local mechanical mixing within the fretting contact.

References

1.   Oladokun, A., M. Pettersson, M. Bryant, H. Engqvist, C. Persson, R. Hall, and A. Neville, *Fretting of CoCrMo and Ti6Al4V alloys in modular prostheses.* Tribology - Materials, Surfaces & Interfaces, 2015. **9**(4): p. 165 - 173.
2.   Baxmann, M.J., S. Y. Schilling, C. Blomer, W. Grupp, T. M. Morlock, M. M., *The influence of contact conditions and micromotions on the fretting behavior of modular titanium alloy taper connections.* Med Eng Phys, 2013. **35**(5): p. 676-83; discussion 676.
3.   Gilbert, J.L., Christine A. Buckley, and Eugene P. Lautenschlager, *Titanium oxide film fracture and repassivation: the effect of potential, pH and aeration*, in *Medical applications of titanium and its alloys*. 1996, ASTM International: The material and biological issues.
4.   Oladokun, A., Michael Bryant, Richard Hall, and Anne Neville, *The effect of cyclic load on the evolution of fretting current at the interface of Metal-on-Metal and Ceramic-on-Metal taper junction of hip prostheses.* Bone Joint J, 2017. **99**(SUPP 5): p. 68-68.
5.   Kawalec, J.S., Stanley A. Brown, Joe H. Payer, and Katharine Merritt, *Mixed-metal fretting corrosion of Ti6Al4V and wrought cobalt alloy.* Journal of Biomedical Materials Research Part A, 1995. **29**(7): p. 867-873.
6.   Brown, S.A., Paula J. Hughes, and Katharine Merritt, *In vitro studies of fretting corrosion of orthopaedic materials.* Journal of orthopaedic research, 1988. **6**(4): p. 572-579.
7.   Uhlig, H.H., et al., *A fundamental investigation of fretting corrosion.* 1953.
8.   Gilbert, J.L., Christine A. Buckley, and Joshua J. Jacobs., *In vivo corrosion of modular hip prosthesis components in mixed and similar metal combinations. The effect of crevice, stress, motion, and alloy coupling.* Journal of biomedical materials research, 1993. **27**(no. 12): p. 1533-1544.
9.   Goldberg, J.R., Gilbert, J. L., Jacobs, J. J., Bauer, T. W., Paprosky, W., & Leurgans, S., *A multicenter retrieval study of the taper interfaces of modular hip prostheses.* Clinical orthopaedics and related research, 2002. **401**: p. 149-161.

10. Royhman, D., Patel, M., Runa, M. J., Wimmer, M. A., Jacobs, J. J., Hallab, N. J., & Mathew, M. T., *Fretting-Corrosion Behavior in Hip Implant Modular Junctions: The Influence of Friction Energy and pH Variation. .* Journal of the Mechanical Behavior of Biomedical Materials, 2016.

11. Porter, D.A., et al., *Modern trunnions are more flexible: a mechanical analysis of THA taper designs.* Clinical Orthopaedics and Related Research®, 2014. **472**(12): p. 3963-3970.

12. Mroczkowski, M.L., et al., *Effect of impact assembly on the fretting corrosion of modular hip tapers.* J Orthop Res, 2006. **24**(2): p. 271-9.

13. Bergmann, G., et al., *Realistic loads for testing hip implants.* Biomed Mater Eng, 2010. **20**(2): p. 65-75.

14. Dyrkacz, R.M.R., J. M. Brandt, J. B. Morrison, S. T. O'Brien, O. A. Ojo, T. R. Turgeon, and U. P. Wyss, *Finite element analysis of the head–neck taper interface of modular hip prostheses.* Tribology International, 2015. **91**: p. 206-213.

15. Banerjee, S., Jeffrey J. Cherian, James V. Bono, Steven M. Kurtz, Rudolph Geesink, R. Michael Meneghini, Ronald E. Delanois, and Michael A. Mont, *Gross trunnion failure after primary total hip arthroplasty.* The Journal of arthroplasty, 2015. **30**(4): p. 641-648.

16. Hall, D.J., Robin Pourzal, Hannah J. Lundberg, Mathew T. Mathew, Joshua J. Jacobs, and Robert M. Urban, *Mechanical, chemical and biological damage modes within head-neck tapers of CoCrMo and Ti6Al4V contemporary hip replacements.* Journal of Biomedical Materials Research Part B, 2017. **Applied Biomaterials**.

17. Hall, D., Robin Pourzal, Craig Della Valle, Jorge Galante, Joshua Jacobs, and Robert Urban, *Corrosion of modular junctions in femoral and acetabular components for hip arthroplasty and its local and systemic effects*, in *In Modularity and Tapers in Total Joint Replacement Devices*. 2015: ASTM International.

18. Rodrigues, D.C., Robert M. Urban, Joshua J. Jacobs, and Jeremy L. Gilbert, *In vivo severe corrosion and hydrogen embrittlement of retrieved modular body titanium alloy hip-implants.* Journal of Biomedical Materials Research Part B, Applied Biomaterials, 2009. **88**(1): p. 206-219.

19. Moharrami, N., et al., *Why does titanium alloy wear cobalt chrome alloy despite lower bulk hardness: A nanoindentation study?* Thin Solid Films, 2013. **549**: p. 79-86.

20. Gilbert, J.L., Mali, S., Urban, R. M., Silverton, C. D., & Jacobs, J. J., *In vivo oxide-induced stress corrosion cracking of Ti-6Al-4V in a neck–stem modular taper: Emergent behavior in a new mechanism of in vivo corrosion.* Journal of Biomedical Materials Research Part B: Applied Biomaterials, 2012. **100**(2): p. 584-594.

21. Skendzel, J.G., J.D. Blaha, and A.G. Urquhart, *Total hip arthroplasty modular neck failure.* J Arthroplasty, 2011. **26**(2): p. 338 e1-4.

22. Dangles, C.J. and C.J. Altstetter, *Failure of the modular neck in a total hip arthroplasty.* J Arthroplasty, 2010. **25**(7): p. 1169 e5-7.

23. Langton, D.J., et al., *Taper junction failure in large-diameter metal-on-metal bearings.* Bone & joint research, 2012. **1**(4): p. 56-63.

24. Bryant, M.G., D. Buente, A. Oladokun, M. Ward, G. Huber, M. Morlock, and A. Neville, *Surface and subsurface changes as a result of tribocorrosion at the stem-neck interface of bi-modular prosthesis.* Biotribology, 2017.

25. Zeng, P., W. M. Rainforth, and R. B. Cook, *Characterisation of the oxide film on the taper interface from retrieved large diameter metal on polymer modular total hip replacements.* Tribology International, 2015. **89**: p. 86-96.

26. Lanting, B.A., Teeter, M. G., Vasarhelyi, E. M., Ivanov, T. G., Howard, J. L., & Naudie, *Correlation of corrosion and biomechanics in the retrieval of a single modular neck total hip arthroplasty design: modular neck total hip arthroplasty system.* The Journal of arthroplasty, 2015. **30**(1): p. 135-140.

27. Fouvry, S., Philippe Kapsa, and Leo Vincent, *Quantification of fretting damage.* Wear, 1996. **200**(1): p. 186-205.

28. Fouvry, S., P. Kapsa, and L. Vincent, *Description of fretting damage by contact mechanics.* ZAMM - Journal of Applied Mathematics and Mechanics / Zeitschrift für Angewandte Mathematik und Mechanik, 2000. **80**(S1): p. 41-44.

29. Bryant, M., Richard Farrar, Robert Freeman, Ken Brummitt, and Anne Neville, *Fretting corrosion characteristics of polished collarless tapered stems in a simulated biological environment.* Tribology International, 2013. **65**: p. 105-112.

30. Hesketh, J., et al., *Biotribocorrosion: Some electrochemical observations from an instrumented hip joint simulator.* Tribology International, 2013. **59**: p. 332-338.

31. Vingsbo, O., and Staffan Söderberg, *On fretting maps.* Wear, 1988. **126**(2): p. 131–147.

32. Fouvry, S. and K. Kubiak, *Development of a fretting–fatigue mapping concept: The effect of material properties and surface treatments.* Wear, 2009. **267**(12): p. 2186-2199.

33. Kirk, A.M., et al., *Debris development in fretting contacts – Debris particles and debris beds.* Tribology International, 2019.

34. Kirk, A.M., et al., *The effect of frequency on both the debris and the development of the tribologically transformed structure during fretting wear of a high strength steel.* Wear, 2019.

35. Swaminathan, V. and J.L. Gilbert, *Fretting corrosion of CoCrMo and Ti6Al4V interfaces.* Biomaterials, 2012. **33**(22): p. 5487-5503.

36. Bryant, M. and A. Neville, *Fretting corrosion of CoCr alloy: Effect of load and displacement on the degradation mechanisms.* Proceedings of the Institution of Mechanical Engineers, Part H: Journal of Engineering in Medicine, 2016. **231**(2): p. 114-126.

37. Clark, E.R., K.E. Porter, and M.G. Bryant, *Fretting-corrosion of cardiovascular stent materials: The role of electrochemical polarisation on debris generation mechanisms.* Biotribology, 2019. **18**: p. 100093.

38. Fischer, A., S. Weiss, and M.A. Wimmer, *The tribological difference between biomedical steels and CoCrMo-alloys.* Journal of the mechanical behavior of biomedical materials, 2012. **9**: p. 50-62.

39. Sauger, E., S. Fouvry, L. Ponsonnet, Ph Kapsa, J. M. Martin, and L. Vincent., *Tribologically transformed structure in fretting.* Wear, 2000. **245**(1): p. 39-52.